RESEARCH ARTICLE

Comparative study of carbon-supported Pd and PdAg catalysts synthesised by the polyol process and reverse micelles methods

**A. J. Armenta-González · R. Carrera-Cerritos ·
M. Guerra-Balcázar · L. G. Arriaga ·
J. Ledesma-García**

Abstract Carbon-supported Pd and PdAg nanoparticles were synthesised by the polyol (P) and reverse micelles (RM) methods for use in a comparative study as catalysts for ethanol electro-oxidation in alkaline media. The electrocatalysts were physically and chemically characterised by transmission electron microscopy, X-ray diffraction and thermogravimetric analysis. Electrochemical characterisation was performed by cyclic voltammetry in the absence and presence of ethanol (0.1, 1, 3 M ethanol), chronoamperometry and electrochemical impedance spectroscopy. The electrochemical measurements showed that the catalysts obtained by the RM method presented excellent dispersion and small crystal size, resulting in materials with high electro-active area. However, the PdAg/C catalysts prepared by the polyol process presented better catalytic activity and stability during the electro-oxidation reaction. In addition to the excellent dispersion and low agglomeration promoted by the polyol method, catalytic enhancement can also be associated with the synergic effect between Pd and Ag elements.

A. J. Armenta-González · L. G. Arriaga (✉)
Centro de Investigación y Desarrollo Tecnológico en
Electroquímica, Parque Tecnológico Querétaro s/n, Sanfandila,
C.P. 76703 Pedro Escobedo, Qro, Mexico
e-mail: larriaga@cideteq.mx

R. Carrera-Cerritos
División de Ciencias Naturales y Exactas, Departamento de
Ingeniería Química, Universidad de Guanajuato, Noria Alta s/n,
Col. Noria Alta, C.P. 36050 Guanajuato, Gto, Mexico

M. Guerra-Balcázar · J. Ledesma-García (✉)
División de Investigación y Posgrado, Facultad de Ingeniería,
Universidad Autónoma de Querétaro, Centro Universitario Cerro
de las Campanas, C.P. 76010 Querétaro, Qro, Mexico
e-mail: janet.ledesma@uaq.mx

1 Introduction

The development of catalysts, such as those ones based on Pd, has been very attractive for many reactions, including the ethanol electro-oxidation reaction (EOR) and the oxygen reduction reaction (ORR) in alkaline medium [1–6]. The main advantages provided by working in alkaline medium are the kinetics acceleration at the electrode and the opportunity to replace the more expensive Pt catalyst commonly used in direct ethanol fuel cells (DEFC) with other cheaper metals, such as palladium [7–11].

Another option usually adopted to decrease the cost of the catalyst for fuel cells is the decrease of Pd loading on the support or through the combination of Pd with other less expensive materials [10–15]. Among various metals capable of combining with Pd, Ag is attractive due to the high synergistic interaction between Pd and Ag. For this reason, Ag has been used as the secondary metal in the preparation of bimetallic electrodes, and hence, has improved catalytic activity in some electrochemical reactions. [16–18]. Different synthesis methods have been used to obtain catalytic materials for the ethanol oxidation reaction in alkaline medium. The catalytic activity of these materials has been investigated, and the apparent activation energy in the PdAg/C catalyst is lower than in pure Pd/C catalyst [19, 20].

The design of anodic electrocatalysts is focused on decreasing the intermediates generated during the oxidation reaction, which significantly decreases the performance of the anode electrode [20–25]. The characteristics of the bimetallic catalysts, such as activity and selectivity, depend on the nature, structure and composition, and they

may be modified during the synthesis procedure [16–25]. For example, obtaining materials via reverse microemulsion provides good control of the nanoparticle size and shape. The exchange of reactants between the micelles in suspension often results in a uniform distribution of the volume into the micelles in the solution, leading to the generation of narrow particle size distribution. In addition, the nanoparticles obtained by reverse micelles (RM) can be synthesised at room temperature, and the surfactants that surround the particles in the suspension can be easily removed [26–30]. On the other hand, the polyol process, which consists of the reduction of metallic precursors by poly-alcohols in the presence of capping ligands, has become widely employed to obtain small nanoparticles with narrow size distribution. However, the presence of capping ligands in the final product is still a problem [31–38]. Following this idea, some catalysts prepared by the polyol (P) and RM methods have been reported, but a direct comparison between these methods has not been made.

The aim of the present work is to synthesise Pd/C and PdAg/C catalysts by the polyol and RM methods to reduce the cost of the electrode anode material and increase the catalytic activity towards EOR. PdAg/C is evaluated at different ethanol concentrations in alkaline medium. The catalysts were structurally characterised by X-ray diffraction (XRD), transmission electron microscopy (TEM) and thermogravimetric (TG) analysis. The electrocatalytic performance was studied by cyclic voltammetry in the absence and presence of ethanol, chronoamperometry and electrochemical impedance spectroscopy (EIS).

2 Experimental methodology

The bimetallic catalysts were prepared at a 1:1 molar ratio (Pd:Ag) and a total metallic load of 30 % on the carbon support.

2.1 Materials

Na_2PdCl_4 (Sigma-Aldrich, 99 %) and $AgNO_3$ (J. T. Baker, 99 %) were the precursors used in both methods. Polyvinylpyrrolidone (PVP) (Sigma-Aldrich), ethylene glycol (EG) (Sigma-Aldrich, 99.8 %) and KBr were employed in the polyol process, whereas hexane (J. T. Baker, 99 %), 2-ethyl-1-hexanol (J. T. Baker, 99 %), Triton X-100 (Sigma-Aldrich, 99.7 %), sodium borohydride (J. T. Baker, 98 %) and ketone (J. T. Baker) were used in the reverse micelles method. All the reactants were used as received without further purification. The P and RM in the catalysts name refer to the corresponding catalyst obtained by the polyol process or reverse micelles, respectively.

2.2 Synthesis of catalysts

The PdAg/C–P catalyst was synthesised using a modified method for obtaining pure Pd nanoparticles [32, 33]. A volume of 5 cm^3 EG was placed in a 25 cm^3 three-neck flask equipped with a reflux condenser and a PTFE-coated magnetic stirring bar. The flask was heated with an oil bath and stirred under static air at constant temperature of 373 K. Meanwhile, 0.024 g of Na_2PdCl_4 and 0.6 g of KBr were dissolved in 3 cm^3 of deionised water and 0.0916 g of polyvinylpyrrolidone, and the corresponding amount of $AgNO_3$ was dissolved in 3 cm^3 of EG at room temperature. The two solutions were then injected simultaneously into the three-neck flask using two syringe pumps at a rate of 45 cm^3 h^{-1}. The reactive mixture was heated at 373 K. After 1 h, Carbon Vulcan XC-72 was added to the reactive mixture and kept at this temperature for 2 h. The reaction was cooled to room temperature and the product was mixed for 24 h, separated by adding 30 cm^3 of ketone and centrifuged at 4,000 rpm for 0.5 h. The final product was washed with water several times by a repetitive dispersion–centrifugation process before drying at 333 K for 12 h. The dried catalyst was heat treated at 540 K for 1 h to remove the impurities. The same process was followed to produce the Pd/C–P catalysts, but in this case, the Ag precursor was not added to the reactor, and the reaction temperature was maintained at 373 K for 1 h.

The Pd/C-RM and PdAg/C-RM catalysts were prepared by a modified method reported previously [9–39]. The reduction of precursor salts was made in partial ionic water in oil microemulsion by a non-ionic surfactant Triton X-100 and a low amount of ionic surfactant sodium dodecylbenzenesulfonate (SDS) and 2-ethyl-1-hexanol as the co-surfactant. These agents were contained in hexane as the oleic phase. The water/surfactant molar ratio was 3:6. The nanoparticles were obtained by mixing two microemulsions with the same composition, one containing the precursor Na_2PdCl_4 0.01 M and the other containing $NaBH_4$ 0.03 M. This mixture was mixed for 1 h until a clear microemulsion was obtained. The amount of Carbon Vulcan XC-72 was calculated to reach a final metal loading of 30 % w/w. This amount of support was added to the mixture under constant magnetic stirring for 24 h at 313 K. The supported catalyst was separated, washed three times with acetone and centrifuged at 4,000 rpm for 15 min. After the separation, the catalyst was washed with deionised water to eliminate surfactant molecules. Finally, a thermal treatment was performed at 540 K for 2 h.

2.3 Characterisation

The crystalline characteristics of the materials were analysed with a Phillips X'Pert XRD instrument, which

provides CuKα radiation. The system was operated at 40 kV and 30 mA, data interval = 1 s and step = 0.0091° from 2θ = 10–90°.

The morphology of the materials was observed on a JEOL JEM-1010 microscope operating at 80 kV and equipped with a tungsten filament as an electron source. The samples were prepared by mixing a small amount of catalyst with ethanol, followed by sonication for 20 min. One drop of the final suspension was dropped over a cupper grid covered by a supporting polymer (formvar). The samples were left to dry for 12 h at room temperature before the TEM session.

The metallic load was measured by TG analysis of the prepared catalyst, which was conducted using a TG balance (TA Instruments, Q500). TG analysis was performed from room temperature to 1,073 K at a heating rate of 10 K min^{-1} under an air flow rate of 60 cm^3 min^{-1}.

Cyclic voltammetry, chronoamperometry and EIS were conducted on a Biologic SAS EPP-400/4000 potentiostat/galvanostat in a three-electrode cell at room temperature. An Hg/HgO in 1 M KOH and a platinum foil electrode were used as the reference electrode and counter electrode, respectively. The working electrode was prepared using a glassy carbon (GC) disc measuring 3 mm in diameter, which was previously polished with alumina powder (0.05 μm), sonicated for 10 min and washed with deionised water. During the electrochemical measurements, a mixture containing 1.0 mg of electrocatalyst and 73 μL of isopropyl alcohol was pretreated under ultrasonication for 20 min. Then, 7 μL of Nafion® solution (5 % isopropyl alcohol, Electrochem) was added to the mixture and sonicated for 20 min to obtain a well-dispersed ink. A volume of 20 μL of the catalyst ink was then transferred onto the surface of the GC electrode and dried in air to obtain a catalyst thin film. Cyclic voltammetry was performed in aqueous solutions of 1 M KOH in both the absence and presence of ethanol solutions of various concentrations from −0.9 to 0.5 V (vs. SHE) at 0.05 V s^{-1}. Before any measurement, the system was bubbled with N$_2$ for 20 min to evacuate the oxygen from the cell. The EIS measurements were recorded from 0.1 Hz to 10 kHz using wave amplitude of 10 mV after the stabilisation of the system for 40 min.

3 Results and discussion

3.1 TEM results

Figure 1 shows the TEM images and particle size distribution of the catalysts studied in the present work. The Pd-particles generated by the polyol method (Fig. 1a) presented a mixture of shapes, including round, cubic and hexagonal, whereas the PdAg/C–P (Fig. 1b) catalyst showed spherical nanoparticles with no observation of agglomeration. The Pd catalyst obtained by the RM method (Fig. 1 c) shows low metal loading onto the carbon support. The PdAg nanoparticles by RM are small and uniformly distributed on the carbon surface; hence, nanoparticle agglomeration was not detected. The main particle sizes of the Pd/C–P, PdAg/C–P, Pd/C-RM, PdAg/C-RM and commercial Pd/C catalysts were estimated to be approximately 5, 8, 7, 3.5 and 5 nm, respectively. The particle size histograms measured from at least 200 nanoparticles present a distribution between 2 and 12 nm for all catalysts prepared, obtaining in the case of PdAg/C-RM the smallest particle size.

3.2 TGA analysis

The organic material due to the residual surfactants, water, solvent and precursors from the synthesis was associated with the weight loss below 623 K (Fig. 2). The weight loss in this region behaved similarly in all catalysts, but the weight loss of the Pd/C–P catalyst in this region was greater than the other catalysts (10 wt % approximately). The significant weight loss, approximately 823 K in all the catalysts, was associated with the carbon dioxide produced by the oxidation of the carbon support with oxygen from the air. The constant weight region at above 873 K was attributed to the residual metal and metal oxide. The metal loading measured was 19, 26, 9, 21 and 19 for the Pd/C–P, PdAg/C–P, Pd/C-RM, PdAg/C-RM and commercial Pd/C catalysts, respectively.

3.3 XRD measurements

Figure 3 shows the XRD patterns of the Pd and PdAg catalysts synthesised by the P and RM methods after annealing at 543 K for 1 h. The catalysts presented broad reflection at 2θ = 25°, which corresponds to the (002) plane of the carbon support. In addition, two peaks centred at $2\theta \sim$ 33.8° and 42° were observed on the commercial Pd/C and PAg/C-RM catalysts; these peaks are likely due to the main reflection of PdO·H$_2$O (JCPDS card 09-0254) given the similar position and relative intensities of the peaks [35]. For the PdAg/C prepared by the polyol process, another two small reflections can be observed at $2\theta \sim$ 30.9 and 44.3°, assigned to the AgBr card. The presence of this compound evidenced the incomplete reduction of the Ag precursor by ethylene glycol and the difficult incorporation of Ag atoms into the Pd structure. However, the reflections with the highest intensity at 2θ = 40.119, 46.659, 68.121 and 82.1 in all the catalysts studied showed face-centred cubic lattice structures corresponding to the (111), (200), (220) and (311) planes of the Pd metallic phase (JCPDS
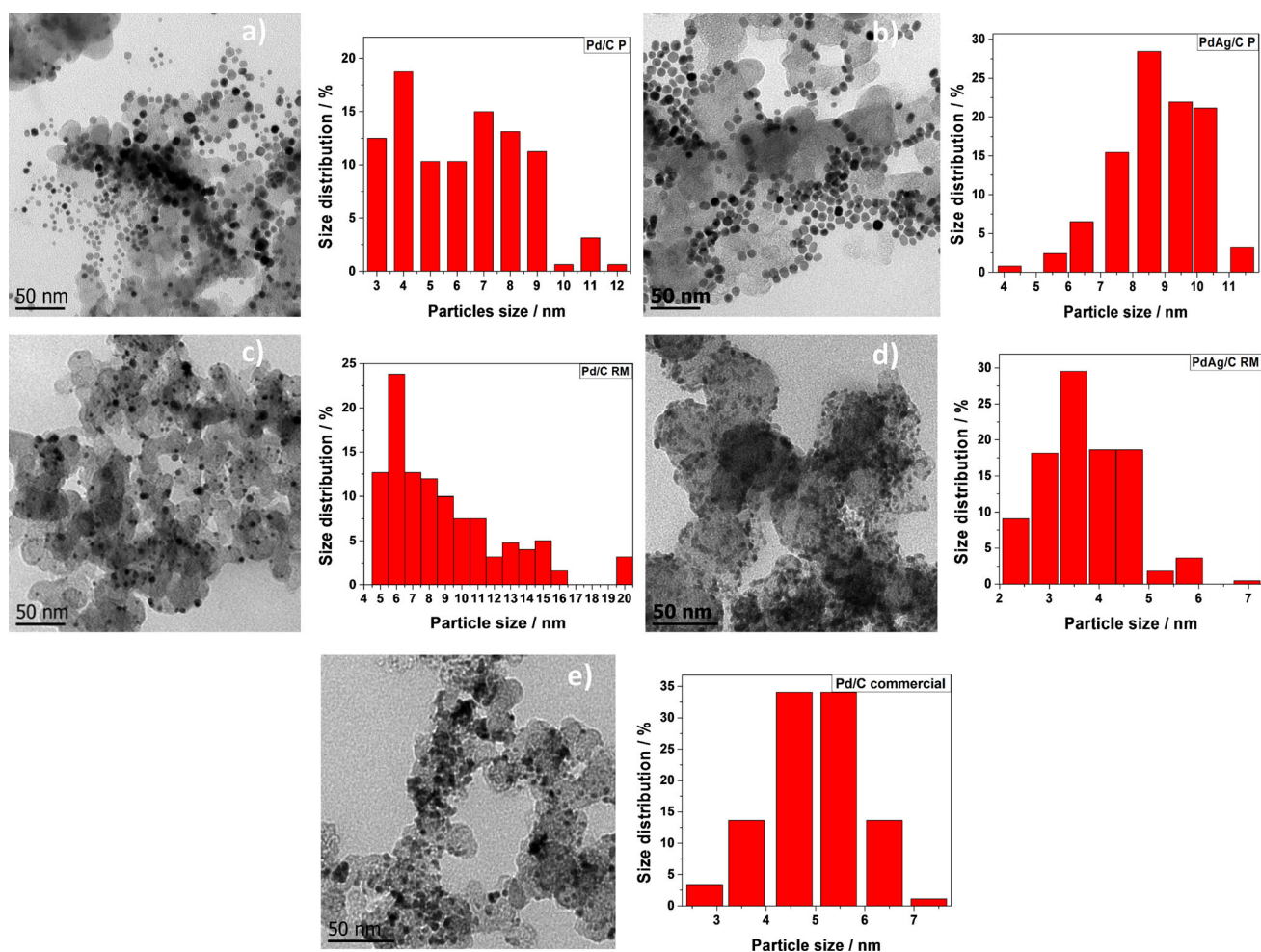
Fig. 1 TEM images and their NPs size distribution of catalysts **a** Pd/C–P, **b** PdAg/C–P, **c** Pd/C-RM, **d** PdAg/C-RM, **e** commercial Pd/C catalyst
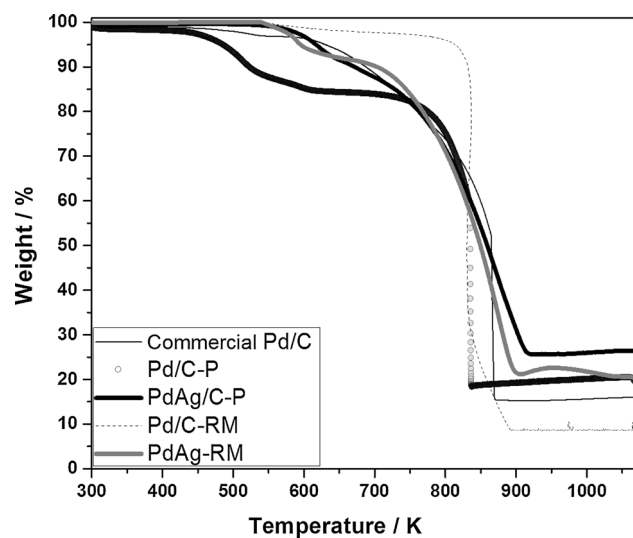

Fig. 2 Weight loss obtained by TGA analysis for the Pd/C–P, PdAg/C–P, Pd/C-RM, PdAg/C-RM and commercial Pd/C catalysts
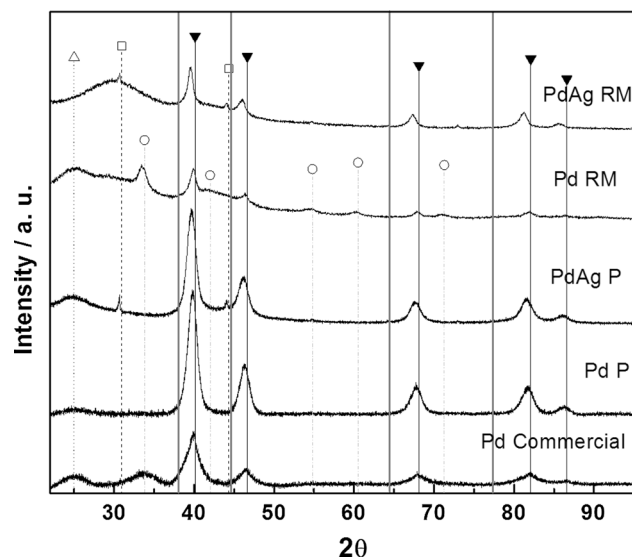

Fig. 3. XRD patterns for the synthesised catalysts (*Black triangles* Pd fcc, *open squares* AgBr, *open triangles* C, *empty circles* PdO)

Table 1 Structural parameters of the synthesised catalysts and commercial Pd/C

	Crystal size, XRD (nm)	Lattice parameter, a (Å)	Main particle size, TEM (nm)	Interplanar distance, d_{111} (Å)	% Ag
Pd polyol	6.2	3.912	5	2.260	–
PdAg polyol	6.4	3.924	8	2.268	≈ 20
Pd commercial	4.8	3.902	5	2.252	–
Pd RM	9.1	3.907	7	2.258	–
PdAg RM	3.2	3.936	3.5	2.275	≈ 30

46-1043), respectively. Pure Ag nanoparticles were not observed in the present study, as the absence of the Ag diffraction peaks demonstrates in Fig. 3 (solid grey line).

The average crystal size and lattice parameter were calculated based on the broadening and position of the (111), (200) and (311) diffraction peaks according to the Scherrer equation and Bragg's law [35]. These values are condensed in Table 1 and are in the same order as those calculated by TEM.

The Pd-reflections of the bimetallic catalysts synthesised by either the P or RM methods shifted towards lower 2θ values compared to that of pure Pd, indicating an expansion of the lattice due to the Ag (larger atom) atoms into the Pd structure (Table 1). The lattice constants of the catalysts calculated from averaging the d-spacing data of (111) (200) and (220) reflections are in the range between the lattice constants of pure Pd and Ag values already reported ($a_{Pd} = 0.389$ nm; $a_{Ag} = 0.409$ nm) [19]. The shifting of the peaks is greater on the PdAg/C-RM compared with the PdAg/C prepared by the polyol process, suggesting an increase in the degree of alloying [31]. Moreover, it has been reported that the alloying degree and composition linearly correlate to the shifting of the peaks in PdAg bimetallic nanoparticles [36]. Under this consideration, the nanoparticle composition was calculated, and the results are shown in Table 1 (PdAg/C–P and PdAg/C-RM rows). These values showed the silver-doped catalysts synthesised by RM had higher silver loading due to the intrinsically higher reductive power of the $NaBH_4$ compared to ethylene glycol.

3.4 Electrochemical characterisation

3.4.1 Cyclic voltammetry

Figure 4 shows the cyclic voltammograms (CV) of the catalysts; the cathodic peak at ~ -0.15 V in the pure-Pd electrodes has been attributed to the reduction of palladium oxides formed during the forward scan. In the case of bimetallic catalysts, the oxidation peaks at anodic potentials are commonly ascribed to the formation of the absorbed hydroxyl OH_{ads}, whereas the peaks at potentials (-0.1 to 0.48 V) are related to the formation of PdO [39].
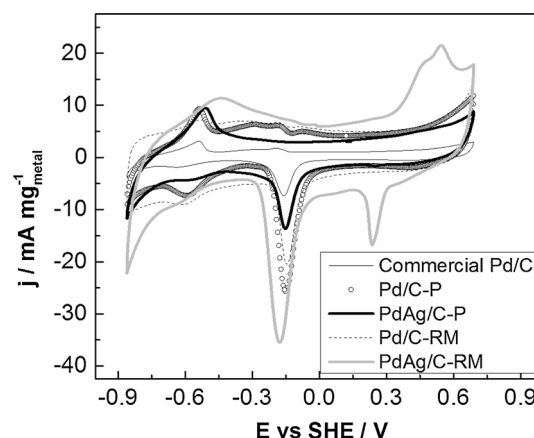

Fig. 4 Cyclic voltammograms of commercial Pd/C, Pd/C–P, PdAg/C–P, Pd/C-RM and PdAg/C-RM electrodes in 1 M KOH

However, on the polarisation curve of the Pd/C-RM catalyst (commercial, P and RM), there is a small peak at ~ 0.6 V in the positive scan where the palladium oxidation cannot be observed clearly. The peak at 0.48 V observed in the PdAg/C-RM catalyst was assigned to the oxidation of the silver (Ag/AgO), which is further reduced at 0.28 V in the negative scan [18]. The electrochemical active surface area (ECSA) of the electrodes has been estimated by determination of the coulombic charge (Q_H) required for the reduction of PdO and using the next relation [40]:

$$\text{ECSA} = \frac{Q_H}{Q_{ref}}, \tag{1}$$

where Q_H is the coulombic charge for the reduction of palladium oxide, and Q_{ref} is a parameter to relate charge with area. A charge value (Q_{ref}) of 405 μC cm^{-2} is assumed for the reduction of the PdO monolayer [41]. The ECSA values in Table 2 were used to normalise the electric current obtained in the CV in the presence of ethanol.
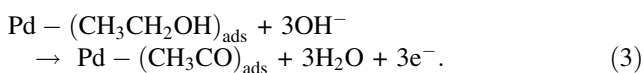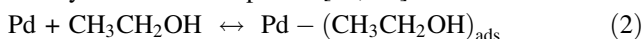
The ECSA values were in the order of PdAg/C-RM > Pd/C–P > Pd/C-RM > PdAg/C–P > commercial Pd/C. The high ECSA can be attributed to a better dispersion and small particle size in the cases of the Pd/C–P and PdAg/C-RM catalysts. The highest surface was for the PdAg/C-RM catalyst, which could be attributed to the small particle size and excellent dispersion observed by TEM.

Table 2 ECSA calculated from Fig. 4

Electrode	Metal loading (mg cm^{-2})	Q_H (μC cm^{-2})	ECSA (cm^2)
commercial Pd/C	0.57	2,822.63	2.84
Pd/C–P	0.6	1,773.7	5.9
PdAg/C–P	0.78	905.12	3.889
Pd/C-RM	0.33	525.5	4.29
PdAg/C-RM	0.70	3,329	9.33

3.4.2 CV in the presence of ethanol

The ethanol electro-oxidation in 1 M KOH of the catalysts is shown in Fig. 5 at three ethanol concentrations. In the anodic scan, the oxidation peak (i_f) was related to the oxidation of freshly chemisorbed species derived from ethanol adsorption, as described by Eq. 2 and 3. The oxidation peak in the reverse scan (i_b) is associated with the removal of carbonaceous species that are not completely oxidised in the anodic scan, rather than the oxidation of freshly chemisorbed species [38, 42]

$$Pd + CH_3CH_2OH \leftrightarrow Pd - (CH_3CH_2OH)_{ads} \quad (2)$$

$$Pd - (CH_3CH_2OH)_{ads} + 3OH^- \\ \rightarrow Pd - (CH_3CO)_{ads} + 3H_2O + 3e^-. \quad (3)$$

The CV shown in Fig. 5 was analysed in terms of the height and position of the peak potential, i_f and E_f,

respectively. In the cases of pure-Pd catalysts, the Pd/C–P catalyst showed the highest i_f value measured from the voltammograms at all ethanol concentrations. In addition, the i_f of the Pd/C-RM catalysts was higher than the commercial one at 1 and 3 M ethanol. The height of the oxidation peak is related to the amount of ethanol reacting at the electrode resulting from the kinetic properties of the catalysts. Under this consideration, the Pd/C–P presented better kinetic performance due to the higher availability of reactive sites, as can be inferred by comparing the electroactive area in Fig. 4. Additionally, the trend observed for E_f was as follows: Pd/C-RM < commercial Pd/C < Pd/C–P at all ethanol concentrations. This result indicates, from a thermodynamic point of view, that the Pd/C-RM catalyst presented a higher activity towards ethanol electro-oxidation compared to the Pd/C catalyst obtained by the polyol process. Moreover, the difference between the E_f values was more significant as the ethanol concentration increased because the oxidation peaks shifted towards more positive potential in all the catalysts. This phenomenon has also been reported in similar Pd catalysts obtained by the polyol process [33]. This behaviour is related to the poisoning of the catalyst.

Regarding the bimetallic catalysts, behaviour similar to the Pd catalysts can be observed. The two PdAg catalysts presented an increase in the current density peak as the ethanol concentration increased. On one hand, the PdAg/C-

Fig. 5 Cyclic voltammetry for the Pd and PdAg catalysts synthesised by the polyol process and reverse micelles method compared with a Pd/C catalyst at **a** 0.1, **b** 1 and **c** 3 M of ethanol
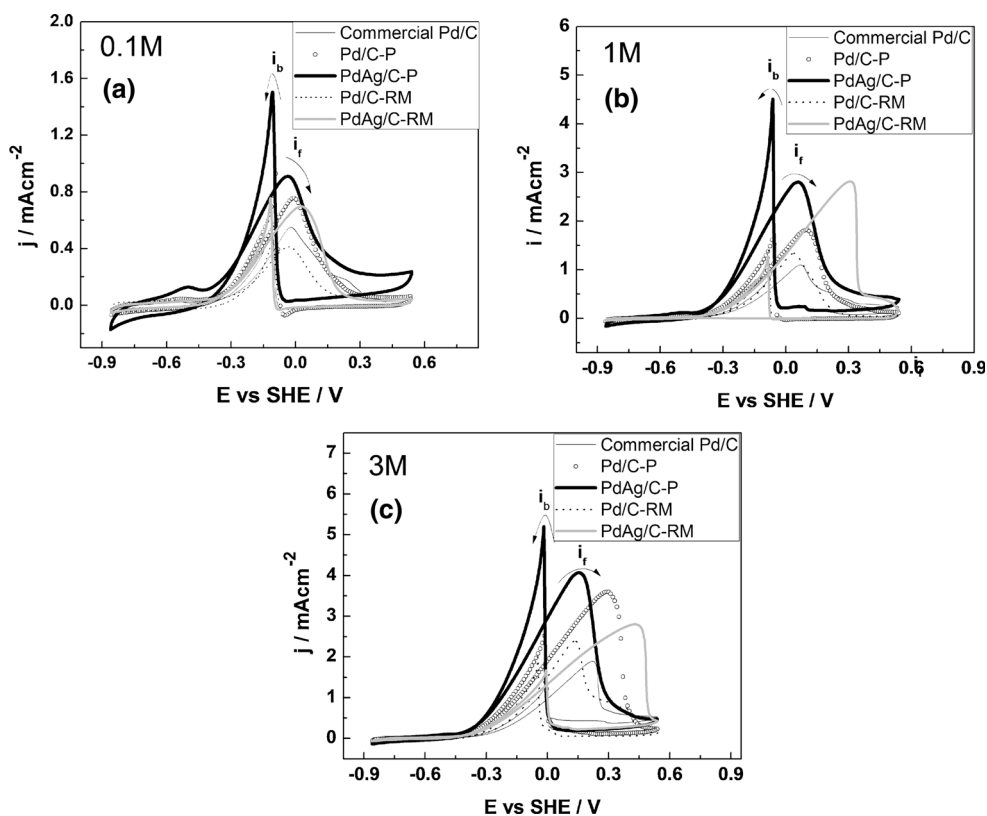
RM catalyst showed a shift towards more positive potential than the bimetallic catalysts synthesised by the polyol process. In fact, the PdAg/C–P catalysts presented a slight change in the peak potential at −35, 51 and 138 mV, at 0.1, 1 and 3 ethanol concentrations, respectively. In contrast, the currents in the negative-going scan for PdAg/C–P are much higher than those in the positive-going scan because the degree of poisoning accumulated on the surface is inferior. On the other hand, the bimetallic catalyst prepared by the polyol process gave the highest i_f at 0.1 and 3 M ethanol concentrations compared with all the analysed catalysts, and a similar height to the peak was observed for the PdAg/C-RM at 1 M, which showed the highest i_f at this concentration. This unexpected behaviour can be explained if we look at Fig. 4. The PdAg catalyst prepared by the RM process showed the highest electro-active area due to the excellent nanoparticle dispersion and smaller nanoparticle size than the PdAg nanoparticles synthesised by the polyol process. Despite this situation, the PdAg/C–P nanocatalyst showed a surface of highly concentrated Pd atoms, and the Ag oxidation/reduction peaks were almost undetected by CV. This lower silver concentration at the PdAg/C catalyst surface and the ease of accessibility to the reactive sites by the reactants due to the low agglomeration observed in TEM images can explain the excellent catalytic properties observed in these materials.

3.4.3 Chronoamperometry

The influence of the synthesis method on the catalytic performance and stability against poisoning was tested by chronoamperometry using the same electrode after CV in the presence and absence of ethanol. Figure 6 shows the lowest current density of commercial Pd/C; the PdAg/C–P catalyst showed not only the best electrocatalytic activity for ethanol oxidation compared to the other catalysts, but it also showed higher efficiency and tolerance to intermediate products during the reaction as the chronoamperometric curve maintained stability along the experiment, which could be explained by the effect between Pd and Ag that removed the poisonous intermediates. This stabilising effect agreed with previously reported observations in PdAg/C catalysts [19]. On the other hand, the catalyst synthesised by RM showed an initial current density comparable to that obtained by the polyol process, but it rapidly decayed in the first 5 min. The excellent catalyst stability of Pd and PdAg prepared by the polyol process could be related to the good morphologic properties observed by TEM and also to the interaction between Ag and Pd in the catalyst. However, for the materials prepared by RM, the poisoning of the catalyst surface can be attributed to other species of Ag and Pd present in the catalyst (AgBr and PdO see Fig. 3) due to the nature of the
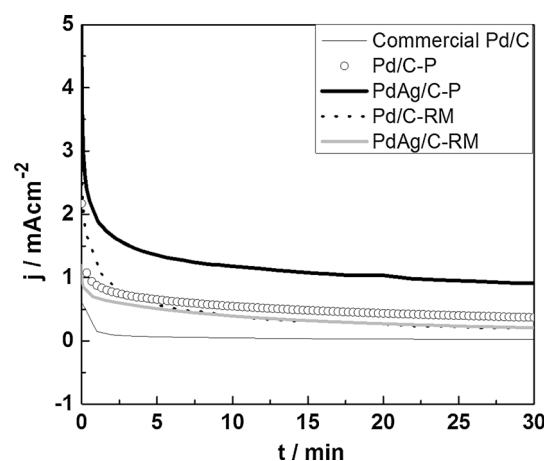

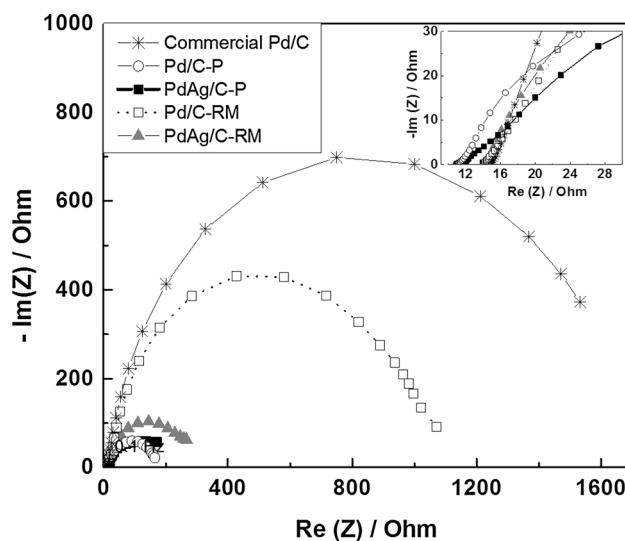**Fig. 6** Chronoamperometry in 1 M ethanol + 1 M KOH at 0.04 V versus SHE

Fig. 7 Impedance spectrum obtained in 1 M KOH + 1 M ethanol solution at 0.04 V versus SHE

synthesis, which could lead to low availability of Ag in the interaction with Pd.

3.4.4 Electrochemical impedance spectroscopy

EIS measurements were performed at 0.04 V versus SHE to compare the impedance characteristics of the electrocatalysts. The corresponding Nyquist plots are shown in Fig. 7. The semicircle at high frequencies (∼10 kHz) represents the charge transfer resistance (R) of the main oxidation reaction. The reaction resistance followed the trend: Pd/C–P < PdAg/C–P < PdAg/C-RM < Pd/C-RM < commercial Pd/C-ME. The smaller charge transfer resistance for the catalysts synthesised by the polyol process is related to the higher catalytic activity observed at this potential (Fig. 5b, 1 M). In the case of PdAg/C-RM, compared with the Pd/C-

RM and commercial Pd catalysts, the small charge transfer resistance could be related to the high homogeneity, small size and high alloying degree of the PdAg/C-RM catalyst.

4 Conclusions

Pd/C and PdAg/C catalysts were successfully synthesised by the P and RM methods, and their activity and stability for the ethanol electro-oxidation reaction in alkaline media were compared. Regarding the Pd materials, the Pd/C–P catalyst showed the highest current density values, whereas the Pd/C-RM catalyst presented a more negative oxidation peak at all ethanol concentrations. The catalysts synthesised by reverse micelles showed excellent dispersion and small particle size that resulted in materials with high electro-active area. However, the bimetallic catalyst prepared by the polyol process (PdAg/C–P) gave the highest current density peaks, the most negative peak potential and the best stability among all the analysed catalysts. In general, this catalytic enhancement in the PdAg/C–P catalyst can be may not only be attributed to the synergic effect between Pd and Ag nanoparticles and good morphologic properties but also to the higher availability of reactive sites and a surface rich in Pd.

References

1. Heshmatpour F, Abazari R, Balalaie S (2012) Preparation of monometallic (Pd, Ag) and bimetallic (Pd/Ag, Pd/Ni, Pd/Cu) nanoparticles via reversed micelles and their use in the Heck reaction. Tetrahedron 68:3001–3011. doi:10.1016/j.tet.2012.02.028

2. Wang X, Wang W, Qi Z, Zhao C, Ji H, Zhang Z (2012) Novel Raney-like nanoporous Pd catalyst with superior electrocatalytic activity towards ethanol electro-oxidation. Int J Hydrog Energy 37:2579–2587. doi:10.1016/j.ijhydene.2011.11.016

3. Bianchini C, Shen PK (2009) Palladium-based electrocatalysts for alcohol oxidation in half cells and in direct alcohol fuel cells. Chem Rev 109:4183–4206. doi:10.1021/cr9000995

4. Jiang LH, Hsu A, Chu D, Chen RR (2009) Oxygen reduction reaction on carbon supported Pt and Pd. J Electrochem Soc 156:B370–B376. doi:10.1149/1.3058586

5. Lima F, Zhang J, Shao MH, Sasaki K, Vukmirovic MB, Ticianelli EA, Adzic RR (2007) Catalytic activity−d-band center correlation for the O$_2$ reduction reaction on platinum in alkaline solutions. J Phys Chem C 111:404–410. doi:10.1021/jp065181r

6. Nie M, Tang H, Wei Z, Jiang SP, Shen PK (2007) Highly efficient AuPd–WC/C electrocatalyst for ethanol oxidation. J Electrochem Commun 9:2375–2379. doi:10.1016/j.elecom.2007.07.006

7. Jiang LH, Hsu A, Chu D, Chen RR (2010) A highly active Pd coated Ag electrocatalyst for oxygen reduction reactions in alkaline media. Electrochim Acta 55:4506–4511. doi:10.1016/j.electacta.2010.02.094

8. Zhiani M, Gasteiger HA, Piana M, Catanorchi S (2011) Comparative study between platinum supported on carbon and non-noble metal cathode catalyst in alkaline direct ethanol fuel cell (ADEFC). Int J Hydrog Energy 36:5110–5116. doi:10.1016/j.ijhydene.2011.01.079

9. Oliveira MC, Rego R, Fernandes LS, Tavares PB (2011) Evaluation of the catalytic activity of Pd–Ag alloys on ethanol oxidation and oxygen reduction reactions in alkaline medium. J Power Sources 196:6092–6098. doi:10.1016/j.jpowsour.2011.03.062

10. Kamarudin MZF, Kamarudin SK, Masdar MS, Daud WRW (2013) Review: direct ethanol fuel cells. Int J Hydrog Energy 38:9438–9453. doi:10.1016/j.hydene.2012.07.059

11. Braunschweig B, Hibbitts D, Neurock M, Wieckowski A (2013) Electrocatalysis: a direct alcohol fuel cell and surface science perspective. Catal Today 202:197–201. doi:10.1016/j.cattod.2012.08.013

12. Yi Q, Niu F, Sun L (2011) Fabrication of novel porous Pd particles and their electroactivity towards ethanol oxidation in alkaline media. Fuel 90:2617–2623. doi:10.1016/j.fuel.2011.03.038

13. Sun S, Jusys Z, Behm RJ (2013) Electrooxidation of ethanol on Pt-based and Pd-based catalysts in alkaline electrolyte under fuel cell relevant reaction and transport conditions. J Power Sources 231:122–133. doi:10.1016/j.jpowsour.2012.12.091

14. Seo MH, Lim EJ, Choi SM, Nam SH, Kim HJ, Kim WB (2011) Synthesis, characterization, and electrocatalytic properties of a polypyrrole-composited Pd/C catalyst. Int J Hydrog Energy 36:11545–11553. doi:10.1016/j.ijhydene.2011.06.070

15. Napoleão Geraldes A, da Silva DF, Segura Pino E, da Silva JCM, de Souza RFB, Hammer P, Vitório Spinace E, Oliveira Neto A, Linardi M, dos Santos MC (2013) Ethanol electro-oxidation in an alkaline medium using Pd/C, Au/C and PdAu/C electrocatalysts prepared by electron beam irradiation. Electrochim Acta 111:455–465. doi:10.1016/j.electacta.2013.08.021

16. Li G, Jiang L, Jiang Q, Wang S, Sun G (2011) Preparation and characterization of Pd$_x$Ag$_y$/C electrocatalysts for ethanol electrooxidation reaction in alkaline media. Electrochim Acta 56:7703–7711. doi:10.1016/j.electacta.2011.06.036

17. Wang Y, Sheng ZM, Yang H, Jiang SP, Li CM (2010) Electrocatalysis of carbon black- or activated carbon nanotubes-supported Pd–Ag towards methanol oxidation in alkaline media. Int J Hydrog Energy 35:10087–10093. doi:10.1016/j.ijhydene.2010.07.172

18. Jin C, Zhang Z, Chen Q, Chen Q (2013) Effect of Ag modification on catalytic activity of Pd electrode for allyl alcohol oxidation in alkaline solution. Electrochim Acta 87:860–864. doi:10.1016/j.electacta.2012.10.014

19. Nguyen ST, Law HM, Nguyen HT, Kristian N, Wang S (2009) Enhancement effect of Ag for Pd/C towards the ethanol electro-oxidation in alkaline media. Appl Catal B 91:507–515. doi:10.1016/j.apcatb.2009.06.021

20. Safavi A, Kazem H, Mameni S, Tohidi M, Khanipour MP (2013) Facile electrocatalytic oxidation of ethanol using Ag/Pd nanoalloys modified carbon ionic liquid electrode. Int J Hydrog Energy 38:3380–3386. doi:10.1016/j.ijhydene.2012.12.040

21. Palma V, Castaldo F, Ciambelli P, Iaquaniello G, Capitani G (2013) On the activity of bimetallic catalysts for ethanol steam reforming. Int J Hydrog Energy 38:6633–6645. doi:10.1016/j.ijhydene.2013.03.089

22. Tang Y, Zhang H, Zhong H, Xu Z (2012) In-situ investigation on the CO tolerance of carbon supported Pd–Pt electrocatalysts with low Pt

content by electrochemical impedance spectroscopy. Int J Hydrog Energy 37:2129–2136. doi:10.1016/j.ijhydene.2011.10.104

23. Waszczuk P, Wieckowski A, Zelenay P, Gottesfeld S, Coutanceau C, Léger JM, Lamy C (2001) Adsorption of CO poison on fuel cell nanoparticle electrodes from methanol solutions: a radioactive labeling study. J Electroanal Chem 511:55–64. doi:10.1016/S0022-0728(01)00559-9

24. Wee JH, Lee KY (2006) Overview of the development of CO-tolerant anode electrocatalysts for proton-exchange membrane fuel cells. J Power Sources 157:128–135. doi:10.1016/j.jpowsour.2005.08.010

25. Pitois A, Pilenga A, Pfrang A, Tsotridis G, Abrams BL, Chorkendorff I (2010) Temperature dependence of CO desorption kinetics at a novel Pt-on-Au/C PEM fuel cell anode. Chem Eng J 162:314–321. doi:10.1016/j.cej.2010.05.002

26. Santos LGRA, Oliveira CHF, Moraes IR, Ticianelli EA (2006) Oxygen reduction reaction in acid medium on Pt–Ni/C prepared by a microemulsion method. J Electroanal Chem 596:141–148. doi:10.1016/j.jelechem.2006.07.033

27. Zhang W, Qiao X, Chen J (2007) Synthesis of silver nanoparticles: effects of concerned parameters in water/oil microemulsion. Mater Sci Eng 142:1–15. doi:10.1016/j.mseb.2007.06.014

28. Venkateswara RC, Viswanathan B (2012) Microemulsion synthesis and electrocatalytic properties of carbon-supported Pd–Co–Au alloy nanoparticles. J Colloid Interface Sci 367:337–341. doi:10.1016/j.jcis.2011.10.020

29. Li L, Huang M, Liu J, Guo Y (2011) Pt$_x$Sn/C electrocatalysts synthesized by improved microemulsion method and their catalytic activity for ethanol oxidation. J Power Sources 196:1090–1096. doi:10.1016/j.jpowsour.2010.08.016

30. Raghuveer V, Ferreira PJ, Manthiram A (2006) Comparison of Pd–Co–Au electrocatalysts prepared by conventional borohydride and microemulsion methods for oxygen reduction in fuel cells. Electrochem Commun 8:807–814. doi:10.1016/j.elecom.2006.03.022

31. Fievet F, Lagier J, Blin B, Beaudoin B, Figlarz M (1989) Homogeneous and heterogeneous nucleations in the polyol process for the preparation of micron and submicron size metal particles. Solid State Ionics 32:198–207. doi:10.1016/0167-2738(89)90222-1

32. Xiong Y, Cai H, Wiley BJ, Wang J, Kim M, Xia Y (2007) Shape-controlled synthesis of Pd nanocrystals and their catalytic applications. Acc Chem Res 129:3665–3675. doi:10.1021/ar300209w

33. Carrera-Cerritos R, Guerra-Balcázar M, Fuentes-Ramírez R, Ledesma-García J, Arriaga LG (2012) Morphological effect of Pd catalyst on ethanol electro-oxidation reaction. Materials 5:1686–1697. doi:10.3390/ma5091686

34. Spirin MG, Brichkin SB, Razumov VF (2005) Synthesis and stabilization of gold nanoparticles in reverse micelles of aerosol OT and Triton X-100. Colloid J 67:485–490. doi:10.1007/s10595-005-0122-4

35. Hu J, Zhou H, Zhang G, Cui Y, Huang L, Xu Y, Chen J, Kuang Y (2010) Investigation on conductivity of mixed surfactants reverse microemulsion. J Appl Electrochem 40:2033–2037. doi:10.1007/s10800-010-0184-9

36. Ghimbeu CM, Zlotea C, Gadiou R, Cuevas F, Leroy E, Latroche M, Vix-Guterl C (2011) Understanding the mechanism of hydrogen uptake at low pressure in carbon/palladium nanostructured composites. J Mater Chem 21:17765–17775. doi:10.1039/C1JM12939B

37. Qi Z, Geng H, Wang X, Zhao C, Ji H, Zhang C, Xu J, Zhang Z (2011) Novel nanocrystalline PdNi alloy catalyst for methanol and ethanol electro-oxidation in alkaline media. J Power Sources 196:5823–5828. doi:10.1016/j.jpowsour.2011.02.083

38. Grden M, Łukaszewski M, Jerkiewicz G, Czerwinski A (2008) Electrochemical behavior of palladium electrode: oxidation, electro-dissolution and ionic adsorption. Electrochim Acta 53:7583. doi:10.1016/j.electacta.2008.05.046

39. Pattabiraman R (1997) Electrochemical investigations on carbon supported palladium catalysts. Appl Catal A 153:9–20. doi:10.1016/S0926-860X(96)00327-4

40. Trasatti S, Petrii O (1991) Real surface area measurements in electrochemistry. Pure Appl Chem 63(5):711–734. doi:10.1351/pac199163050711

41. Singh RN, Singh A, Anindita (2009) Electrocatalytic activity of binary and ternary composite films of Pd, MWCNT, and Ni for ethanol electro-oxidation in alkaline solutions. Carbon 47:271–278. doi:10.1016/j.carbon.2008.10.006

42. Liang ZX, Zhao TS, Xu JB, Zhu LD (2009) Mechanism study of the ethanol oxidation reaction on palladium in alkaline media. Electrochim Acta 54:2203–2208. doi:10.1016/j.electacta.2008.10.034